Vibration of a Helicopter Planetary Gear: Experiments and Analytical Simulation

Tristan M. Ericson

Department of Mechanical and Aerospace Engineering

Ohio State University

Columbus, Ohio 43210

ericson.15@osu.edu

March 4, 2011

Abstract

Planetary gear vibration is a major source of noise and may lead to fatigue-induced failures in bearings or other drivetrain components. Gear designers use mathematical models to analyze potential designs, but these models remain unverified by experimental data. This paper presents experiments that completely characterize the dynamic behavior of a planetary gear by modal testing and spinning tests under operating conditions, focusing on the independent motion of planetary components. Accelerometers are mounted directly to individual gear bodies. Rotational and translational accelerations obtained from the experiments are compared to the predictions of a lumped parameter model. Natural frequencies and modes agree well. Forced response also agrees well between experiments and the model. Rotational, translational, and planet mode types presented in published analytical research are observed experimentally.

INTRODUCTION

Planetary gears are used in many commercial and military applications: helicopters, automobiles, wind turbines, agricultural equipment, and more. They usually transmit high loads, leading to increased noise and vibration. Excessive vibration may cause failures at the gears or propagate through bearings to the surrounding drivetrain components and housing. Several computer models are presented in the research literature [1–6] that allow engineers to predict the dynamic behavior of planetary gear designs. These models, however, are not verified by controlled experiments that demonstrate the independent motion of planetary gear components.

Early planetary gear research focused on analytical models of spur gears, studying the relationship between natural frequencies and system parameters. Cunliffe et al. [1] explored the characteristics of vibration modes in a 13 degree-of-freedom planetary gear with a fixed carrier. Botman [2] studied the modes of an 18 degree-of-freedom system and the effects of planet pin stiffness on the natural frequencies. August and Kasuba [3] used a 9 degree-of-freedom model to compare the performance of fixed versus floating sun gears and argue that a fixed sun gear system with accurate gearing outperforms a floating sun system. Saada and Velex [4] presented a model for planetary gears with spur or helical gears. Abousleiman et al. [7] later included flexibility of the ring gear and carrier. Kahraman [5] proposed a simplified lumped parameter model, providing closed-form expressions for torsional natural frequencies in terms of system parameters. Bahk and Parker used analytical and computational methods to find nonlinear behavior in an equally spaced spur planetary gear [8]. Assuming a symmetric system with even load sharing, Lin and Parker [6] showed that a two-dimensional planetary system has unique modal properties. They classified all modes into three types, each with distinct characteristics: *rotational*, *translational*, and *planet* modes.

Finite element methods are also used to study planetary gear dynamics. Abousleiman and Velex [9] developed a hybrid three-dimensional finite element/lumped parameter model and used it to analyze planetary gear dynamics with a flexible annulus and planet carrier [7]. Vijayakar [10] developed a specialized finite element/contact mechanics program that permits a relatively coarse mesh near the contact region to allow dynamic solution. Parker et al. [11] and Ambarisha and

Parker [12] used this tool to analyze a planetary gear, showing strong correlation with an analytical lumped parameter model.

Experimental work on planetary gear dynamics has not kept pace with theoretical research. Some experiments are conducted under static or quasi-static conditions [13]. Schlegel and Mard [14], Toda and Botman [15], and Platt and Leopold [16] all investigated the effects of planet spacing, planet position error, or tooth numbers on vibration amplitudes. They showed that the dynamic response is particularly sensitive to these factors, which impact the symmetry of the system. The most extensive studies were published in a series of papers by Hidaka et al. [17–20], who showed that loads may not be distributed equally among the planets at high speed, even when they are balanced at quasi-static speeds [17].

This research independently measures the dynamic response of each planetary gear. Experiments with this level of detail have not been published in the literature, but they are necessary to validate computer models and provide practical industry design guidance. The experimental results presented in this paper will increase confidence in–or expose weaknesses of–current simulation tools and serve as a reference for future modeling and design efforts.

EXPERIMENTAL SETUP

Two types of experiments are performed to characterize the dynamic behavior of a test planetary gear. *Modal tests* apply a static torque while a modal hammer or vibration shaker excites the loaded system. Custom-made fixtures constrain one of the planetary shafts with a load cell while static torque is applied to the other shaft. The system frequency response is calculated from the measured input and output signals. *Spinning tests* are performed under representative operating conditions. A drive motor rotates the gears through their operating speed range while a dynamometer applies load. Torque is held constant while the speed is gradually increased or decreased. Lubrication temperature is also held constant.

Test Stand

Figure 1 shows the test stand in the modal testing configuration. A load cell at the end of a radial arm (A) fixes the sun gear shaft to the bedplate. An excitation arm (B) is connected to the carrier shaft where a vibration shaker (shown in photograph) or modal hammer excites the system. A compliant coupling (C) isolates the system from the torque actuator (D).

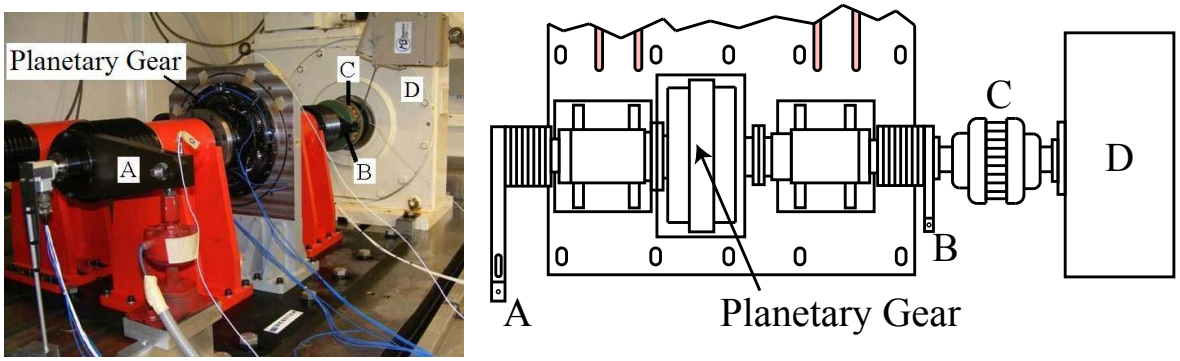

(a) (b)

Figure 1: PLANETARY GEAR MODAL TESTING SETUP (a) PHOTOGRAPH AND (b) SCHEMATIC SHOWING (A) LOAD CELL ARM FIXING INPUT SHAFT TO BEDPLATE, (B) EXCITATION ARM, (C) COMPLIANT COUPLING TO ISOLATE GEARBOX FROM (D) TORQUE ACTUATOR.

Figure 2 shows the test stand in the spinning configuration. A straightforward direct drive system eliminates signal contamination that may occur from the reaction gearbox in a power re-circulation setup. A 250 hp (186 kW) motor not shown at (A) drives the system. Grooved V-belts (B) offset the gearbox from the axis of the drive motor and dynamometer to allow room for slip rings (C) on the input and output shafts to collect data from spinning instrumentation. Using the belts in this manner has an added benefit: they serve as a mechanical filter, isolating the test article from the drive motor and dynamometer. Custom pulleys (D) are attached to the input/output shafts. Four spherical thrust roller bearings (E) support each shaft. The test gearset (F) is contained inside a housing (G). Planet slip rings (H) used to transmit data from transducers mounted directly to the planet gear are contained inside a custom carrier. An optional compliant coupling (J) is not

used in these experiments[1]. Precise location of the planetary gear components is necessary in the absence of system compliance from flexible or floating supports, but the more constrained system may be preferred if necessary precision exists [3]. The 150 hp (112 kW) load dynamometer at (K) provides load. The symmetric nature of the test fixtures permits inversion of the test gear to drive the sun gear or carrier. The ring gear is grounded to the gearbox housing in either configuration.

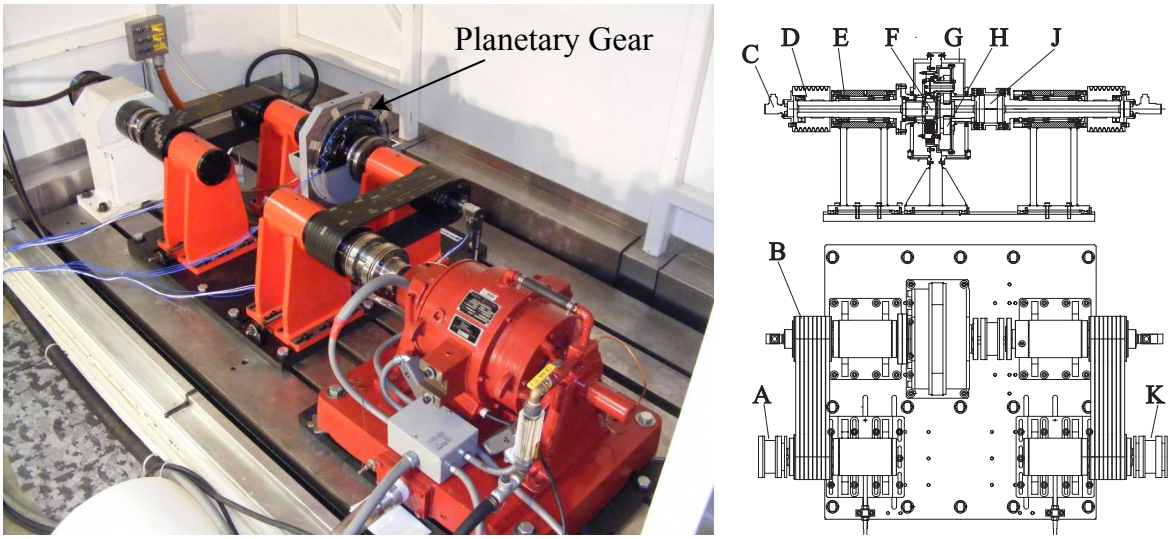

(a) (b)

Figure 2: PLANETARY GEAR SPINNING TEST CONFIGURATION (a) PHOTOGRAPH AND (b) SCHEMATIC DIAGRAM OF PLANETARY GEAR TEST RIG. (A) INPUT FROM DRIVE MOTOR, (B) POWER TRANSMISSION BELTS, (C) END-OF-SHAFT SLIP RINGS, (D) PULLEYS, (E) SPHERICAL THRUST ROLLER BEARINGS (FOUR PER SHAFT), (F) PLANETARY TEST ARTICLE, (G) GEARBOX HOUSING/GUARDS, (H) PLANET SLIP RING, (J) OPTIONAL COMPLIANT COUPLING, (K) OUTPUT TO LOAD DYNAMOMETER.

[1]The coupling adds compliance to compensate for manufacturing errors, but the weight of cantilevered components is too great to permit its use.

Test Article

Table 1 gives the basic dimensions of the planetary gear test article. Spur gears restrict motion to two dimensions. A finite element program [10] shows that root stresses and static tooth deflections are similar to practical gear operating levels for the torques used in the experiments.

Measuring the independent motion of all gear bodies is a primary objective in the experiments. Several carrier features provide instrumentation access. Carrier components were carefully machined to minimize errors in planet pin locations that may disrupt load sharing [21]. Accelerometer adapters were manufactured and bolted directly to the sun and planet gears.

Table 1: BASIC PLANETARY GEAR DIMENSIONS.

	Sun gear	Planet gears (5)	Ring gear
Number of teeth	32	41	118
Pressure angle (*deg*)	25		17.07
Center distance (*mm*)		89.66	
Diametral pitch (*mm*)		262.64	
Diameters (*mm*)			
Base	71.25	91.29	262.71
Root	72.92	92.56	285.32
Tip	84.48	104.60	274.80

Instrumentation

Rotational and translational vibrations of rotating bodies (carrier, sun gear, and two of five planets) are measured using four tangentially-mounted accelerometers. The sensors are rigidly connected to the gear bodies near the meshing teeth to ensure measurement reliability. Figure 3 shows the tangentially-mounted carrier accelerometers and radially-mounted ring gear accelerometers. Ring accelerometers are used to detect radial elastic deformation as observed experimentally by Hidaka et al. [18] and theoretically analyzed by Wu and Parker [22], although the ring gear is bolted to a large fixed housing with sixteen bolts to achieve a nearly-rigid connection, which is assumed by many mathematical models [5,6]. Figure 4 shows the accelerometers mounted to the planet gears. This is an innovative aspect of these experiments, as no previously published studies have directly measured planet gear vibration.

To acquire the data from the planet gear accelerometers (Fig. 4) during spinning tests, two slip rings are required: one to transmit data from the planet reference frame to the carrier reference frame and another from the carrier frame to ground. Figure 2(b) shows both of these slip rings. Once transmitted to the carrier frame through (H), the planet signals travel with the carrier accelerometer wires through the hollow shaft to the slip ring at (C).

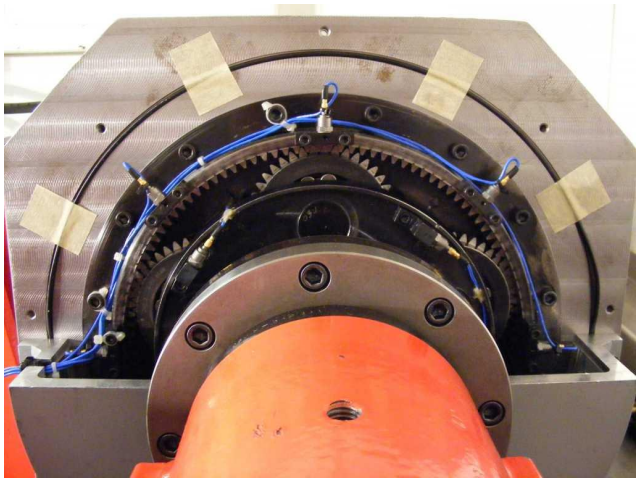

Figure 3: ACCELEROMETERS MOUNTED TO RING GEAR AND CARRIER.

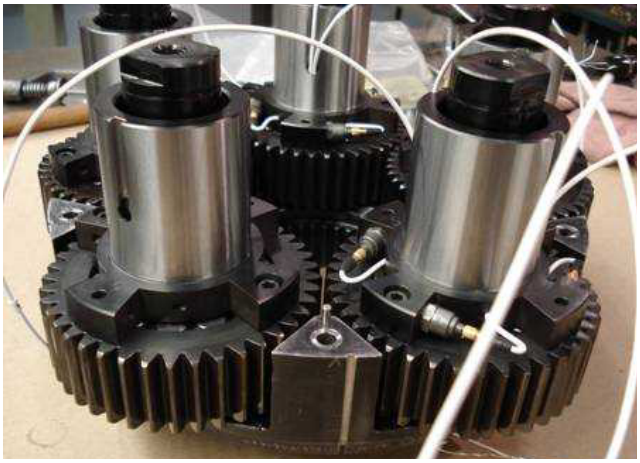

Figure 4: PLANET ACCELEROMETERS ATTACHED TO RIGID ADAPTER FLANGE.

Rotational acceleration can be obtained without knowing the instantaneous orientation of the instrumented gears while the system is spinning. Translational accelerations, however, require knowledge of the instantaneous gear position during data collection, so encoders track the position of each instrumented gear body. Encoders are built into the two end-of-shaft slip rings shown in Fig. 2(b) at (C), and the planet slip rings at (H) have encoders to measure planet position respect to the carrier. The ten-channel slip ring on the sun gear shaft has a 512 *ppr* encoder, and the 36-channel slip ring on the carrier shaft has a 1,024 *ppr* encoder. The eight-channel planet slip rings have 1,024 *ppr* encoders. All encoders operate in quadrature to obtain the highest degree of precision. Each unit has a once-per-rev indexing pulse that defines the nominal orientation of the gear body and establishes a reference with the accelerometer mounting locations.

Data Acquisition

Twenty one accelerometers and four encoders simultaneously track the motion of all planetary gear components during spinning tests. Torque is monitored at the drive motor and dynamometer shafts. An analog tachometer signal is measured at either the input or output shaft, although the encoders accurately measure gear speed and mesh frequency. Plotting the overall RMS of measured data at each speed does not provide insightful data. Several mesh harmonics excite many natural frequencies, rendering individual peaks indistinguishable. The frequency spectra through-

out the speed range shows low amplitude vibration away from mesh frequency harmonics, so order tracking isolates vibrations at each harmonic, making is easier to identify natural frequencies and understand the dynamic response.

Data processing of modal tests is straightforward. The gear is stationary; its orientation is known and constant, so the encoders are not needed. Static torque is measured at the sun gear shaft. Impulse tests use standard techniques to calculate frequency response from the measured time signals. Shaker tests apply a sine sweep excitation. There is only one excitation frequency at each sweep step, so order tracking is not necessary. The acceleration response RMS is normalized by the applied force RMS at each frequency step.

LUMPED PARAMETER MODEL

The analytical formulation presented by Lin and Parker [6] is the foundation of the model used to analyze the experimental system. Rotational and translational vibrations of all gear bodies, as well as rotation of the two pulleys (D in Fig. 2(b)) connected by the sun and carrier shafts are considered. Figure 5(a) shows the model for modal tests with load cell and excitation arm inertias added to the pulleys and grounded by the appropriate stiffnesses. Figure 5(b) shows the lumped parameter model for the spinning tests with the belts connecting the pulleys to ground. Figure 6 shows the details of the planetary gear model that is common to both setups. Gear vibrations are measured with respect to the kinematically rotating carrier reference frame $\{\mathbf{e}_i^c\}$. The orientation of this reference basis is given by the carrier encoder and rotates with constant carrier speed $\dot{\theta}_c$ in spinning tests. The gear is stationary for modal tests with constant offset angle $\theta_c = -19.8^\circ$ with respect to the ground basis $\{\mathbf{E}_i\}$. The location of the N planets on the carrier reference frame is θ_{pn}, $n = 1,...,N$. For the test case under study, $N = 5$ and θ_{pn} = [-20, 52, 124, 196, 268]. Further details of the planetary gear model are given in [6].

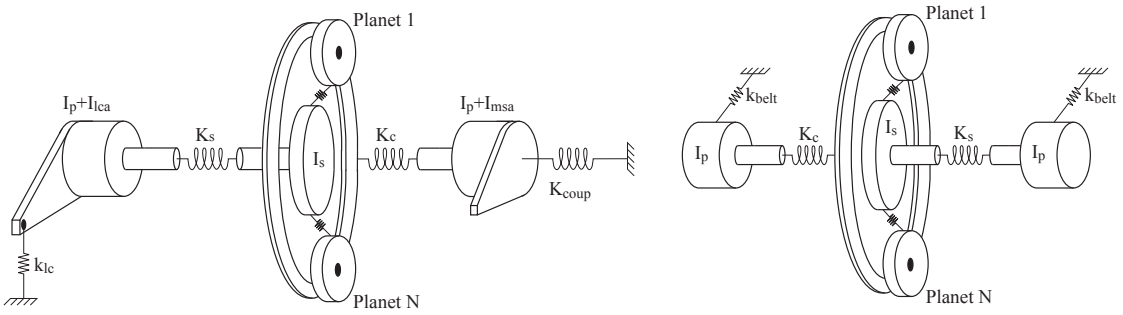

(a) (b)

Figure 5: OVERALL LUMPED PARAMETER MODEL OF (a) MODAL TESTS WITH THE LOAD CELL ARM GROUNDING THE SUN PULLEY AND COMPLIANT COUPLING GROUNDING THE CARRIER PULLEY, AND (b) SPINNING TESTS WITH BELTS GROUNDING EACH PULLEY.

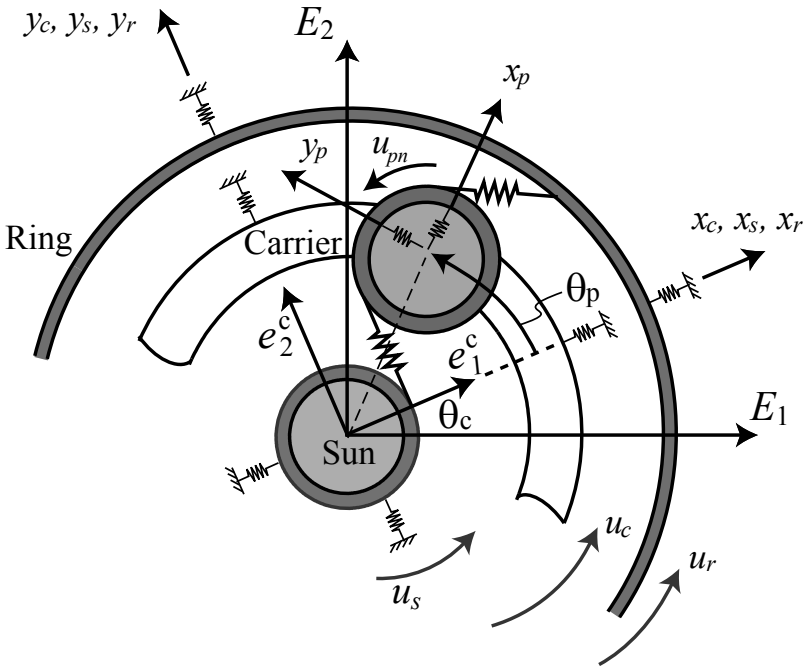

Figure 6: LUMPED PARAMETER MODEL OF PLANETARY GEAR WITH VIBRATIONS MEASURED ON THE CARRIER REFERENCE FRAME ROTATING WITH CONSTANT ANGULAR SPEED $\dot{\theta}_c$.

The analytical model gives the matrix equation of motion with the associated displacement vector $\mathbf{q}$ as

$$\begin{aligned} &\mathbf{M}\ddot{\mathbf{q}} + \mathbf{C}\dot{\mathbf{q}} + [\mathbf{K}_m + \mathbf{K}_v(t)]\mathbf{q} = \mathbf{f} \\ &\mathbf{q} = (u_{p1},\ \mathbf{q}_{ring},\ \mathbf{q}_{sun},\ \mathbf{q}_{carrier},\ \mathbf{q}_{planet1}, \ldots,\ \mathbf{q}_{planetN}, u_{p2})^T \\ &\mathbf{q}_i = (x_i, y_i, u_i) \\ &\text{where } i = \textit{ring, sun, carrier, planet1, ..., planet N} \end{aligned} \tag{1}$$

This equation neglects the skew-symmetric gyroscopic matrix containing Coriolis acceleration terms proportional to carrier velocity and centripetal acceleration terms in the stiffness matrix. The effect of these quantities is negligible at operating test speeds. Experimental post-processing that neglects Coriolis and centripetal terms shows insignificant deviations from post-processing that accounts for them. The stiffness matrix $\mathbf{K}$ is divided into a mean component $\mathbf{K}_m$ and a vibrating component $\mathbf{K}_v(t)$. $\mathbf{K}_m$ contains bearing stiffness and mean mesh stiffness terms, while $\mathbf{K}_v(t)$ includes only the fluctuating mesh stiffness. $\mathbf{f}$ is the applied external load. For all experiments in this paper, the applied preload torque at the sun gear is 150 $N \cdot m$ (110 $ft \cdot lb_f$) with a reaction torque at the carrier. This was the maximum possible torque in spinning tests, which was limited by the capabilities of the drive motor, dynamometer, and belts. For consistency, the same torque is applied in modal tests, although experiments at higher and lower torques did not significantly affect the dynamic response in modal testing.

The analytical model shows that symmetry conditions inherent to planetary gears lead to three types of modes [6]: *rotational*, *translational*, and *planet* modes. Rotational modes are characterized by purely rotational motion of the central members (sun gear, carrier, and ring gear). Translational modes are defined by purely translational motion of the central members. Planet modes are characterized by motion in the planet gears only.

Modal Test Modeling

The experimental setup is stationary during modal testing, so the mesh stiffness is constant and $\mathbf{K}_v(t) = 0$. Mesh stiffness is proportional to the number of teeth in contact. The contact ratio of this planetary gear is low. Most gear meshes will be in single tooth contact, although it is difficult to observe each mesh cycle position because of the small backlash and difficulty of visually inspecting each mesh once the test is assembled and preload torque is applied. An estimation of each mesh stiffness is applied based upon the stiffness profile over one mesh cycle.

The applied force is the preload torque plus the excitation force of the impact hammer or shaker. The applied preload torque, however, causes a static deflection that the accelerometers do not detect. A transformation is applied so that $\mathbf{z} = \mathbf{q} - \mathbf{q}_m$, where $\mathbf{q}_m$ is the mean value of $\mathbf{q}$. $\mathbf{z}$ is the dynamically fluctuating component of the original displacement vector $\mathbf{q}$. Equation (1) then reduces to

$$\mathbf{M}\ddot{\mathbf{z}} + \mathbf{C}\dot{\mathbf{z}} + \mathbf{K}_{mt}\mathbf{z} = \mathbf{f}_{mt} \tag{2}$$

$\mathbf{f}_{mt}$ is the applied excitation from the impact hammer or shaker only. The equation of motion is linear, and frequency domain analysis is easily performed. Impulse tests with the impact hammer striking the tip of the radial excitation arm (B in Fig. 1) cause an applied translational force and moment which is modeled at the pulley where the excitation arm is attached. For shaker tests, a sinusoidal rotational and/or translational input is applied to the appropriate degrees-of-freedom, depending on the location of the shaker attachment point. The shaker was attached to the planet gear body along the line of action with the ring gear to apply a combined force/moment in tests presented later in this paper.

Spinning Test Modeling

The transformation introduced above, $\mathbf{q} = \mathbf{z} + \mathbf{q}_m$, is applied to the spinning test system. The static case gives $\mathbf{f}_{preload} = \mathbf{K}_m \mathbf{q}_m$. The parametric excitation $\mathbf{K}_v(t)\mathbf{z}$ on the left hand side is ignored. This leads to the equation of motion for spinning tests as

$$\mathbf{M}\ddot{\mathbf{z}} + \mathbf{C}\dot{\mathbf{z}} + \mathbf{K}_m \mathbf{z} = -\mathbf{K}_v(t)\mathbf{q}_m \tag{3}$$

The excitation on the right hand side is the product of the fluctuating mesh stiffness matrix $\mathbf{K}_v(t)$ and the mean deflection $\mathbf{q}_m = \mathbf{K}_m^{-1}\mathbf{f}_{preload}$.

The fluctuating mesh stiffness matrix $\mathbf{K}_v(t)$ requires the variation in sun-planet and ring-planet mesh stiffness for each of the five sun-planet and ring-planet mesh pairs. A finite element model [10] gives the mesh stiffness variation for one reference sun-planet and one reference ring-planet mesh. The mesh phasing relationships developed in [23] give the phase difference between the reference mesh and the remaining four meshes. Figure 7 shows the mesh stiffness variations used to construct $\mathbf{K}_v(t)$. Frequency domain analysis uses the complex form of the excitation -$\mathbf{K}_v(t)\mathbf{q}_m$ to compare the response to different mesh frequency excitation harmonics with the experimental data processed by order tracking.

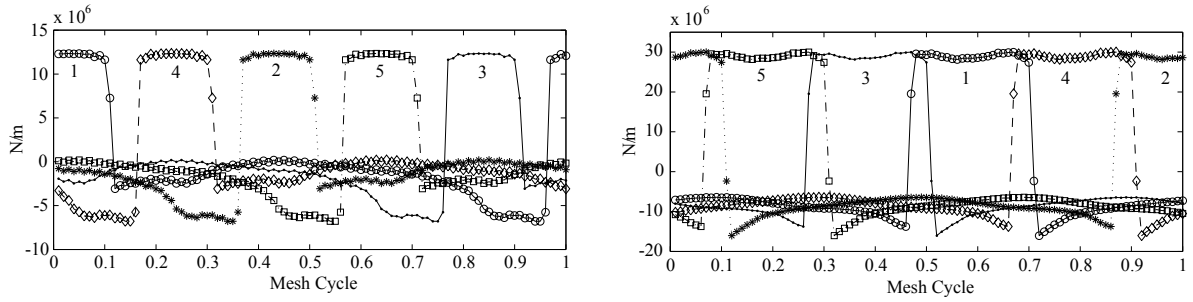

(a) (b)

Figure 7: FLUCTUATING PORTION OF MESH STIFFNESS OF (a) FIVE SUN-PLANET MESHES AND (b) FIVE RING-PLANET MESHES OVER ONE MESH CYCLE WITH 150 $N \cdot m$ PRELOAD TORQUE FOR EXPERIMENTAL PLANETARY GEAR INDICATING MESH PHASE ORDER.

MODAL TESTING

Impact and shaker excitation are used in modal testing. Initial experiments use the load cell arm (A) and the excitation arm (B) as shown in Fig. 1 as impact excitation points. Data from these tests agrees well with the analytical model below 1,000 Hz, but the high-frequency modes have small deflection at the chosen excitation point, so correlation at higher frequencies is poor. The analytical model shows that modes below 1,000 Hz have significant strain energy in the shafts and kinetic energy in the carrier, sun gear, and pulleys (where the impacts are applied). They have negligible strain energy in the gear meshes and negligible kinetic energy in the planet gears. Modes above 1,000 Hz tend to have the opposite: significant strain energy in the tooth meshes, high kinetic energy in planetary gear components, and low deflection at the load cell and excitation arms. Modes below 1,000 Hz are called *fixture modes* because they are characterized by deflection in system components: shafts, pulleys, and the entire planetary gear as a lumped quantity. Modes above 1,000 Hz are called *gear modes* because they are predominantly characterized by motion of the individual planetary gear components. Figure 8 shows the strain energy distribution among the system components in a typical low-frequency fixture mode and a high-frequency gear mode. Like other fixture modes, shaft deflection dominates the 396 Hz mode. Like other gear modes, mesh deflection and planet bearing deflection dominate the 1,831 Hz mode. Both modes shown in Figure 8 are rotational modes. Impact testing on the excitation arm (B in Fig. 1) is used to analyze the fixture modes. Subsequent shaker tests, with excitation directly on a planet gear, reveal the gear modes.

Impact Testing

Figure 9 shows the frequency response of carrier rotation to an impulse at the load cell arm in the low-frequency range. The model and experiments agree well in this region of fixture modes dominated by strain energy in the shafts and kinetic energy in the pulleys. This impact minimally excites the high-frequency gear modes, which contain negligible deflection at the impact point. The 178 Hz peak shown in the experiments corresponds with a translational mode in the model. It

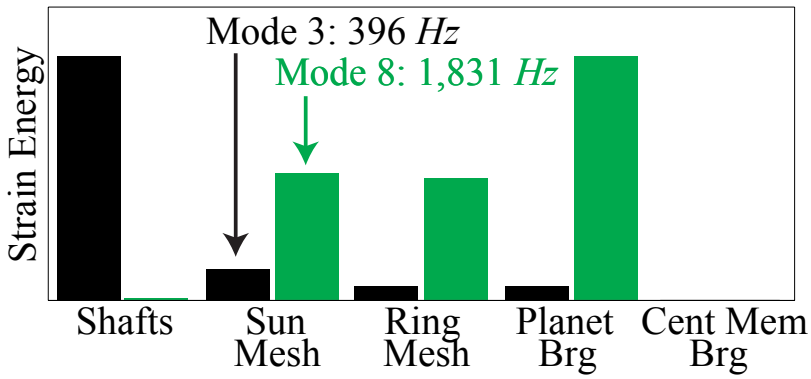

Figure 8: ANALYTICAL MODEL STRAIN ENERGY DISTRIBUTION IN A ROTATIONAL *FIXTURE MODE* (396 Hz) AND A ROTATIONAL *GEAR MODE* (1,831 Hz).

is not expected to appear in carrier rotation and suggests that there is some blending of mode types. Alternatively, this peak may correspond to a natural frequency of the torque actuator, which might exhibit a low-frequency rotational mode with its high inertia. The torque actuator is not modeled because its dynamics would be well below the target frequency range.

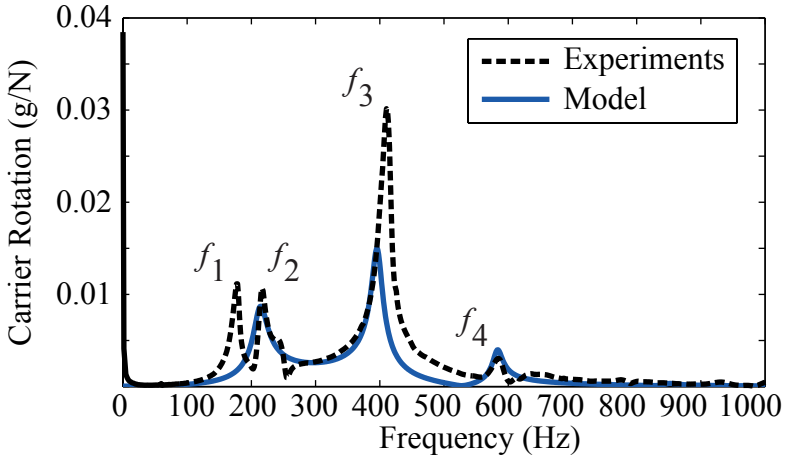

Figure 9: FREQUENCY RESPONSE OF CARRIER ROTATION TO AN IMPACT AT THE LOAD CELL ARM: EXPERIMENTAL MEASUREMENT AND ANALYTICAL MODEL PREDICTION. PRELOAD TORQUE IS 150 $N \cdot m$ AT THE SUN GEAR.

Shaker Testing

The analytical model predicts significant decoupling between the low-frequency shaft modes and the high-frequency gear modes. Impact testing at the radial arms (A and B in Fig. 1) provides good agreement among the low-frequency modes, but it is more desirable to correlate the high-frequency modes that contain significant gear mesh deflection. An MB Dynamics Modal 50 (222 N) shaker is mounted directly to a planet gear along its line of action with the ring gear as shown in Figure 10. A controlled speed sweep excites the planetary gear. The excitation voltage to the shaker is adjusted to maintain a constant force amplitude at the excitation point. Greater excitation magnitudes reveal better dynamic response, especially in system components further away from the excitation point. An MB Dynamics SS250VCF amplifies a sinusoidal signal generated from an HP 33120A function generator. The data acquisition computer running LabVIEW controls the incremental excitation frequency and amplitude of the function generator signal. A proportional controller determines the excitation voltage amplitude based upon measurements in previous frequency steps. With this process, 22 N (5 lb_f) is the maximum excitation amplitude obtained throughout the entire target frequency range containing the high-frequency modes characterized by significant gear mesh deflection, namely, 1,500 to 3,500 Hz.

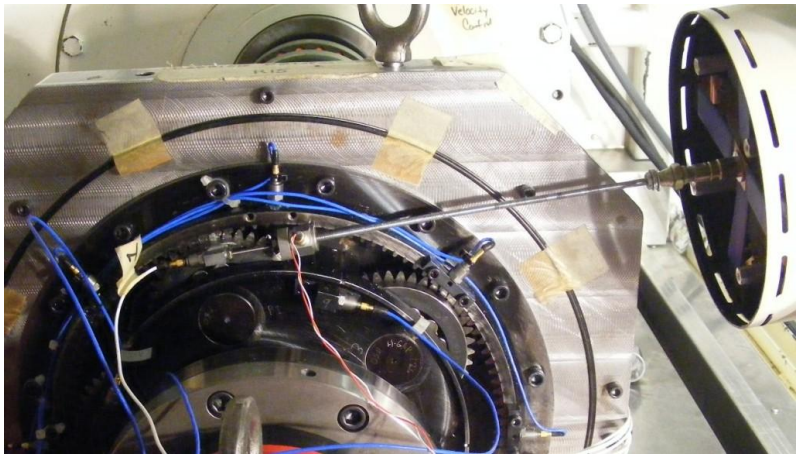

Figure 10: MODAL TESTING SETUP WITH 50 lb_f (222 N) SHAKER ATTACHED DIRECTLY TO A PLANT GEAR ALONG THE LINE OF ACTION WITH THE RING GEAR. ACTUAL INPUT FORCE IS MEASURED AT THE CONTACT POINT.

Excellent correlation with the analytical model is obtained with these controlled experiments. The model predicts nine natural frequencies in this range: three rotational modes, three translation modes, and three planet modes. Translational and planet modes have a multiplicity of two. Table 2 compares *all* of the natural frequencies of the planetary gear set obtained from impact testing and shaker testing[2]. The dynamic response measured in experiments and the eigenvectors of the model identify the nature of the modes. The three mode types predicted by Lin and Parker [6] are noticeable in the experiments. Modes are numbered in increasing order per the analytical model, which coincides with the experiments except for two cases. The horizontal line separates the low-frequency shaft modes below 1,000 Hz (impact testing) from the high-frequency gear modes above 1,000 Hz (shaker testing). Two modes at very high frequency associated with the rigid mounting of the ring gear are not shown.

Model parameters are *not* tuned to match experimental natural frequencies in Tab. 2. These results use the baseline parameters that are physically measured (masses and bearing stiffnesses) or estimated by finite element models (moments of inertia and mesh stiffnesses). Twelve of the fifteen modes agree within 5%. The error in modes seven and nine may trace back to the number of teeth actually in contact at each mesh. With a low contact ratio, the model assumes single tooth contact for each mesh pair. Figure 7, however, shows that there will be one ring-planet mesh pair in double tooth contact and possibly one sun-planet mesh pair in double tooth contact at any point in the mesh cycle. Inability to know which mesh pairs are in double tooth contact may lead to this error. Subsequent spinning tests, with mesh stiffnesses averaged over a mesh cycle, show better agreement in these modes.

[2]Omitting structural modes of the housing or carrier in experiments.

Table 2: NATURAL FREQUENCIES OF TEST GEAR: MODAL TESTING AND ANALYTICAL MODEL. IMPACT TESTS AT THE EXCITATION ARM DETERMINE MODES BELOW 1,000 Hz. SHAKER TESTS (Fig. 10) DETERMINE MODES ABOVE 1,000 Hz.

Mode	Type	Modal Testing	Model	Error
1	*Trans*	178 Hz	176 Hz	-1%
2	*Rot*	217 Hz	214 Hz	-1%
3	*Rot*	411 Hz	396 Hz	-4%
4	*Rot*	586 Hz	583 Hz	-1%
5	*Trans*	660 Hz	682 Hz	3%
6	*Rot*	840 Hz	849 Hz	1%
7	*Planet*	2,186 Hz	1,791 Hz	-18%
8	*Rot*	1,893 Hz	1,831 Hz	-3%
9	*Trans*	2,228 Hz	1,914 Hz	-14%
10	*Planet*	2,477 Hz	2,363 Hz	-5%
11	*Rot*	2,230 Hz	2,399 Hz	8%
12	*Trans*	2,556 Hz	2,470 Hz	-3%
13	*Planet*	2,667 Hz	2,704 Hz	1%
14	*Rot*	2,761 Hz	2,808 Hz	2%
15	*Trans*	2,868 Hz	2,809 Hz	-2%

Figure 11 shows the frequency response in planet rotation during the shaker tests described. The locations and amplitudes of resonant peaks agree well. Figures 12 and 13 show the frequency response in sun gear and carrier translation, respectively. The X- and Y-translations are measured on the rotating carrier reference frame $\{\mathbf{e}_i^c\}$ (Fig. 6). Relative amplitudes of the natural frequencies agree well among all degrees-of-freedom. The biggest difference is the location, and in some cases amplitude, of f_9. Taking into consideration all of the natural frequencies shown in these figures among all the degrees-of-freedom (including those not shown) and their relative amplitudes, however, the comparisons establish significant confidence in the model.

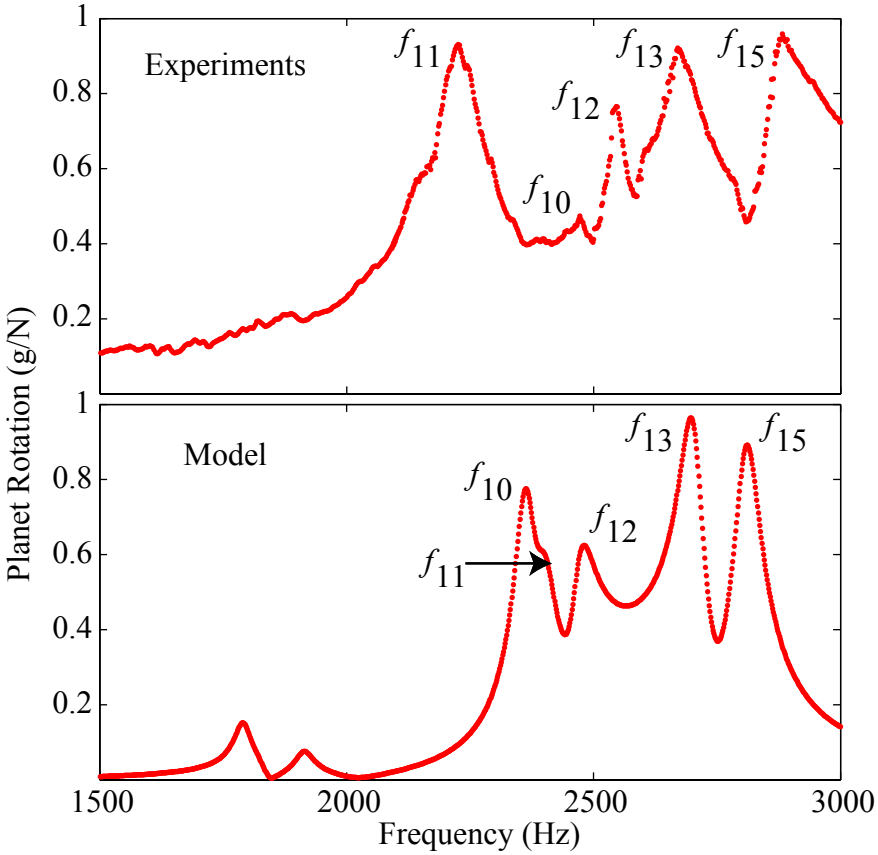

Figure 11: FREQUENCY RESPONSE OF PLANET ROTATION COMPARING EXPERIMENTS TO THE LUMPED PARAMETER MODEL. SHAKER EXCITATION ON THE PLANET GEAR BODY ALONG THE LINE OF ACTON WITH THE RING GEAR. STATIC PRELOAD TORQUE IS 150 $N \cdot m$ AT THE SUN GEAR.

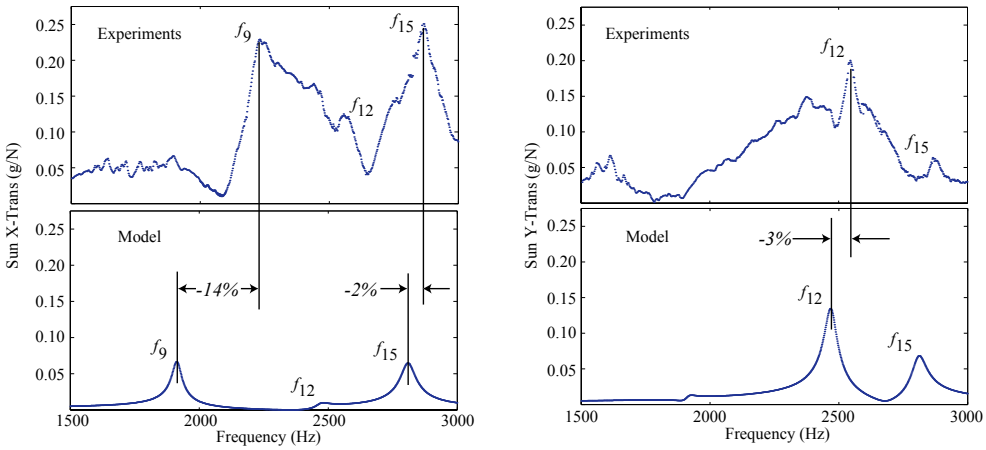

(a) (b)

Figure 12: FREQUENCY RESPONSE OF SUN GEAR TRANSLATION WITH SHAKER EXCITATION ON THE PLANET GEAR BODY ALONG THE LINE OF ACTON WITH THE RING GEAR, COMPARING EXPERIMENTS TO THE LUMPED PARAMETER MODEL IN THE (a) X- AND (b) Y-COORDINATE ON THE ROTATING CARRIER REFERENCE FRAME $\{\mathbf{e}_i^c\}$.

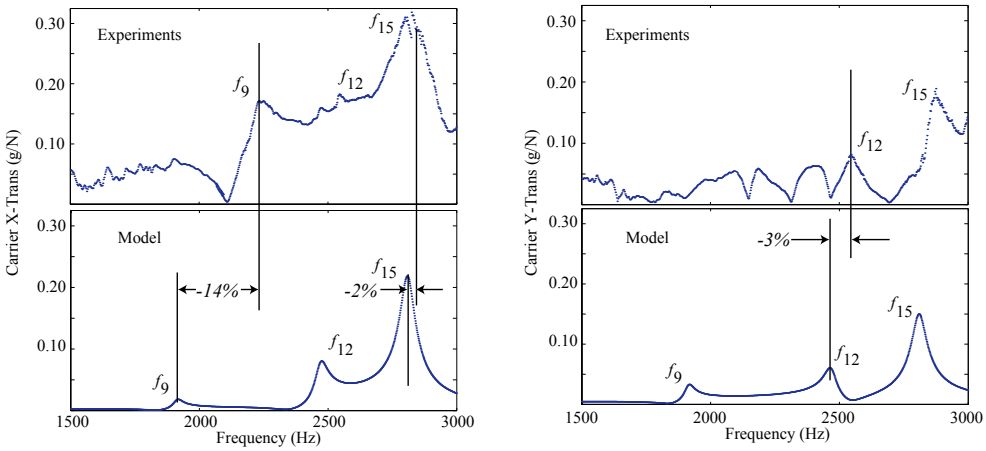

(a) (b)

Figure 13: FREQUENCY RESPONSE OF CARRIER TRANSLATION WITH SHAKER EXCITATION ON THE PLANET GEAR BODY ALONG THE LINE OF ACTON WITH THE RING GEAR, COMPARING EXPERIMENTS TO THE LUMPED PARAMETER MODEL IN THE (a) X- AND (b) Y-COORDINATE ON THE ROTATING CARRIER REFERENCE FRAME $\{\mathbf{e}_i^c\}$.

SPINNING TESTING

Data obtained from spinning tests has higher damping, so it may be difficult to differentiate neighboring modes. The results, however, clearly support modal testing data and correlation with the model. The analytical model predicts three groups of gear modes with similar natural frequencies above 1,500 Hz, each containing one planet mode, one rotational mode, and one translational mode. In this region it may be difficult to discriminate natural frequencies grouped closely together, but the location of high amplitude response agrees with the model. Data at the lower end of the frequency range is quite clear.

The distinct rotational, translational, and planet mode types revealed naturally in the analytical model were present in the preceding discussion on modal testing. These modes are also identified in spinning tests. Planet modes appear at higher frequencies near other modes and, therefore, are difficult to distinguish in spinning tests.

Rotational Modes

Rotational modes are characterized by purely rotational motion of the central members. Figure 14 shows five natural frequencies detected in rotation of the carrier and sun gear. These natural frequencies do *not* appear in translational degrees-of-freedom. Order tracking separates out the response to the first five harmonics of mesh excitation so the natural frequencies and modes can be examined. Vibration amplitude is plotted against response frequency, so resonant peaks appear at the natural frequencies regardless of the harmonic number. The first and second harmonic of mesh frequency do not excite modes above 1,500 Hz due to speed limitations of the experiments.

The low-frequency shaft modes below 1,000 Hz tend to feature predominant response in one degree-of-freedom. Experiments show that carrier rotation dominates modes 3 and 4, whereas sun rotation dominates mode 5. The analytical model is in agreement. Table 3 compares the rotational modes identified in spinning tests with the analytical model prediction. The natural frequencies differ from those presented in the modal testing setup because the boundary conditions have changed (Fig. 5) and the mean mesh stiffness over one mesh cycle is used. Parameter values with uncertain

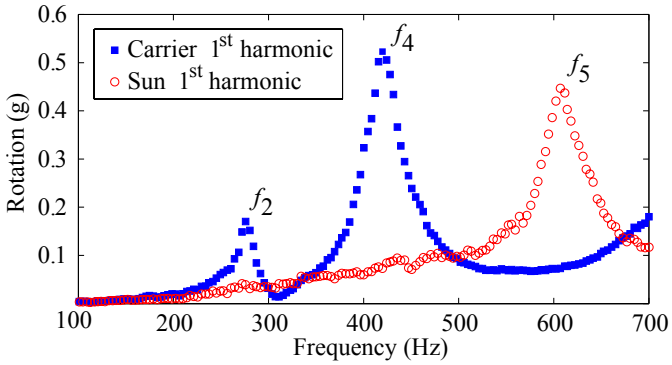

(a)

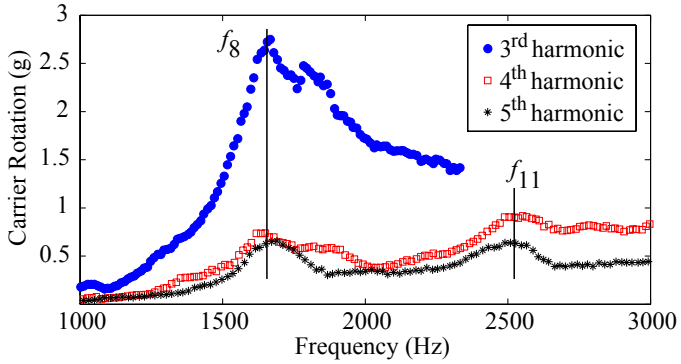

(b)

Figure 14: DYNAMIC RESPONSE OF PLANETARY GEAR ROTATIONAL MOTION DURING SPINNING TESTS WITH ORDER TRACKING. (a) 1^{st} HARMONC OF CARRIER AND SUN GEAR. (b) 3^{rd} THROUGH 5^{th} HARMONC OF CARRIER ROTATION. STATIC PRELOAD TORQUE IS 150 $N \cdot m$ AT THE SUN GEAR.

accuracy are allowed to vary (typically less than 20%) to match the low-frequency modes. The lowest and highest modes predicted by the model are not confirmed in spinning tests, but mode 14 is strongly confirmed in modal testing. Experiments show some low-amplitude response near the first mode predicted by the model, but a natural frequency in the motor and a natural frequency in the dynamometer are found in this region, so speculation is avoided. Four of the five modes agree below 10% error, the other at 13%.

Table 3: ROTATIONAL MODES OF TEST GEARSET: SPINNING TESTS AND ANALYTICAL MODEL. STATIC PRELOAD TORQUE IS 150 $N \cdot m$ AT THE SUN GEAR.

Mode	Spinning Tests	Model	Error
1	-	113 Hz	
3	283 Hz	320 Hz	-13%
4	426 Hz	413 Hz	-3%
5	629 Hz	641 Hz	2%
8	1,672 Hz	1,828 Hz	9%
11	2,548 Hz	2,395 Hz	-6%

Translational Modes

Translational modes are characterized by translational motion of the central members. Figure 15 shows three natural frequencies detected in translation of the carrier that are predicted by the analytical model (f_2, f_6, and f_9). These modes are apparent in the sun gear as well, but plotting sun and carrier response on the same graph was not convenient because sun translation is high in mode 6 compared to the other peaks. The second harmonic is used in Fig. 15(a) because response amplitudes are higher than the first harmonic. This is consistent with predictions of mesh phasing, which indicate that translational response is minimized in the first, fourth, and fifth harmonics. Rotational modes identified above are *not* excited in translational degrees-of-freedom. A finite element model of the gearbox housing shows two modes in the vicinity of the 277 Hz and 474 Hz natural frequencies in Fig. 15(a) that the analytical model does not capture. The 1,464 Hz natural frequency is near a few structural modes identified by a finite element model of the carrier.

Table 4 compares the translational modes identified in spinning tests with the analytical model prediction. As with the rotational modes presented above, some parametric tuning was allowed to match the low-frequency modes. No tuning was performed to match the high-frequency modes. Experiments identify two peaks in the high-frequency range, as illustrated in Fig. 15(b). The 1,949

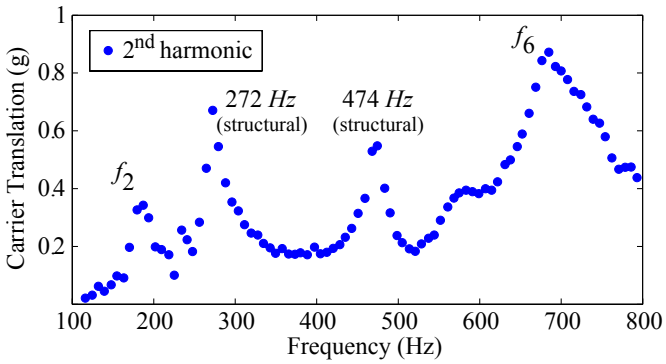

(a)

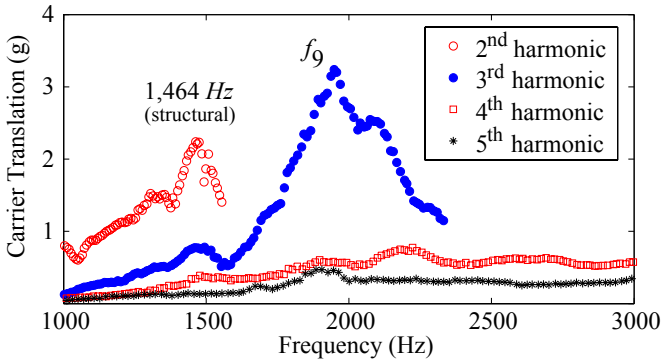

(b)

Figure 15: DYNAMIC RESPONSE OF CARRIER TRANSLATIONAL MOTION DURING SPINNING TESTS WITH ORDER TRACKING. (a) 2^{nd} HARMONC OF CARRIER Y-TRANSLATION. (b) 2^{nd} THROUGH 5^{th} HARMONC OF CARRIER Y-TRANSLATION. STATIC PRELOAD TORQUE IS 150 $N \cdot m$ AT THE SUN GEAR.

Hz peak probably corresponds to mode 9 in the model. This interpretation assumes that the 1,464 Hz peak is a structural mode of the carrier housing and the higher harmonics of mesh frequency do not excite the highest two natural frequencies of the model. (Mesh phasing predicts minimized response in the fourth and fifth harmonics, which in any case, have low excitation amplitudes.) If the 1,464 Hz peak is actually mode 9 and the 1,949 Hz peak is mode 12, the error would be 32% and 27%, respectively.

Table 4: TRANSLATIONAL MODES OF TEST GEARSET: SPINNING TESTS AND ANALYTICAL MODEL. STATIC PRELOAD TORQUE IS 150 $N \cdot m$ AT THE SUN GEAR.

Mode	Spinning Tests	Model	Error
2	180 Hz	174 Hz	-3%
-	272 Hz	structural	
-	474 Hz	structural	
6	670 Hz	671 Hz	0%
-	1,464 Hz	structural	
9	1,949 Hz	1,926 Hz	-1%
12	-	2,477 Hz	
15	-	2,839 Hz	

CONCLUSIONS

Modal testing and spinning tests conducted under operating conditions experimentally measured the natural frequencies and dynamic response of a production planetary gear. Sensors mounted directly to each component give the independent motions of each gear body (sun gear, carrier, and two planets). Post-processing resolves rotational and translational vibrations. Natural frequencies and dynamic response are compared to predictions of an analytical model. Without tuning the model parameters, modal tests confirm all natural frequencies predicted in the model; twelve of fifteen agree within 5%. Dynamic response–including vibration amplitude–is also confirmed across the frequency range in nearly every degree-of-freedom. Spinning tests further confirm many of the natural frequencies that the model predicts. The existence of rotational, translational, and planet mode types (particularly the former two) predicted in the literature is verified experimentally. Separation of low-frequency shaft modes below 1,000 Hz and high-frequency tooth deflection modes is demonstrated in the experiments and the model.

ACKNOWLEDGEMENT

This research was conducted under the guidance of Prof. Robert Parker, director of the Dynamics and Vibrations Lab in the Mechanical and Aerospace Engineering Department of The Ohio State University. The project was funded by the Vertical Lift Consortium and the National Rotorcraft Technology Center, Aviation and Missile Research, Development and Engineering Center under Technology Investment Agreement W911W6-06-2-0002, entitled National Rotorcraft Technology Center Research Program. The authors would like to acknowledge that this research and development was accomplished with the support and guidance of the NRTC, VLC, US Army Research Office, and Ohio State University. The views and conclusions contained in this document are those of the authors and should not be interpreted as representing the official policies, either expressed or implied, of the Aviation and Missile Research, Development and Engineering Center or the U.S. Government.

References

[1] Cunliffe, F., Smith, J. D., and Welbourn, D. B., 1974. "Dynamic tooth loads in epicyclic gears". *ASME Journal of Engineering for Industry,* ***95***(2), May, pp. 578–584.

[2] Botman, M., 1976. "Epicyclic gear vibrations". *Journal of Engineering for Industry,* ***98***(3), Aug., pp. 811–815.

[3] August, R., and Kasuba, R., 1986. "Torsional vibrations and dynamic loads in a basic planetary gear system". *Journal of Vibration, Acoustics, Stress, and Reliability in Design,* ***108***(3), July, pp. 348–353.

[4] Saada, A., and Velex, P., 1995. "An extended model for the analysis of the dynamic behavior of planetary trains". *Journal of Mechanical Design,* ***117***(2), June, pp. 241–247.

[5] Kahraman, A., 1994. "Natural modes of planetary gear trains (letters to the editor)". *Journal of Sound and Vibration,* ***173***(1), pp. 125–130.

[6] Lin, J., and Parker, R. G., 1999. "Analytical characterization of the unique properties of planetary gear free vibration". *Journal of Vibration and Acoustics,* ***121***(3), July, pp. 316–321.

[7] Abousleiman, V., Velex, P., and Becquerelle, S., 2007. "Modeling of spur and helical gear planetary drives with flexible ring gears and planet carriers". *Journal of Mechanical Design,* ***129***, Jan., pp. 95–106.

[8] Bahk, C.-J., and Parker, R. G., 2011. "Analytical solution for the nonlinear dynamics of planetary gears". *Journal of Computational and Nonlinear Dynamics,* ***2***(6), April.

[9] Abousleiman, V., and Velex, P., 2006. "A hybrid 3d finite element/lumped parameter model for quasi-static and dynamic analyses of planetary/epicyclic gear sets". *Mechanism and Machine Theory,* ***41***(6), June, pp. 725–748.

[10] Vijayakar, S. M., 1991. "A combined surface integral and finite-element solution for a three-dimensional contact problem". *International Journal for Numerical Methods in Engineering,* ***31***(3), Mar., pp. 525–545.

[11] Parker, R. G., Agashe, V., and Vijayakar, S. M., 2000. "Dynamic response of a planetary gear system using a finite element/contact mechanics model". *Journal of Mechanical Design,* ***122***(3), Sept., pp. 304–310.

[12] Ambarisha, V. K., and Parker, R. G., 2007. "Nonlinear dynamics of planetary gears using analytical and finite element models". *Journal of Sound and Vibration,* ***302***(3), May, pp. 577–595.

[13] Kahraman, A., 1999. "Static load sharing characteristics of transmission planetary gear sets: Model and experiment". *SAE Transactions,* ***108***, pp. 1954–1963.

[14] Schlegel, R. G., and Mard, K. C., 1967. "Transmission noise control approaches in helicopter design". In ASME Design Engineering Conference, no. 67-DE-58.

[15] Toda, A., and Botman, M., 1980. "Planet indexing in planetary gears for minimum vibration". *ASME*(79-DET-73).

[16] Platt, R. L., and Leopold, R. D., 1996. "A study on helical gear planetary phasing effects on transmission noise". In VDI Berichte, no. 1230, pp. 793–807.

[17] Hidaka, T., Terauchi, Y., and Nagamura, K., 1976. "Dynamic behavior of planetary gear (1st report, load distribution in planetary gear)". *Bulletin of JSME,* ***19***(132), June, pp. 690–698.

[18] Hidaka, T., Terauchi, Y., and Ishioka, K., 1976. "Dynamic behavior of planetary gear (2nd report, displacement of sun gear and ring gear)". *Bulletin of the JSME,* ***19***(138), Dec., pp. 1563–1570.

[19] Hidaka, T., Terauchi, Y., and Ishioka, K., 1979. "Dynamic behavior of planetary gear (4th report, influence of the transmitted tooth load on the dynamic increment load)". *Bulletin of the JSME,* ***22***(167), June, pp. 877–884.

[20] Hidaka, T., Terauchi, Y., and Nagamura, K., 1979. "Dynamic behavior of planetary gear (6th report, influence of meshing-phase)". *Bulletin of the JSME,* ***22***(169), July, pp. 1026–1033.

[21] Ma, P., and Botman, M., 1985. "Load sharing in a planetary gear stage in the presence of errors and misalignment". *Journal of Mechanisms, Transmissions, and Automation in Design - Transactions of the ASME,* ***107***(Sp. Iss.), Mar., pp. 4–10.

[22] Wu, X., and Parker, R. G., 2008. "Modal properties of planetary gears with an elastic continuum ring gear". *Journal of Applied Mechanics,* ***75***(3), May, pp. 1–10.

[23] Parker, R. G., and Lin, J., 2004. "Mesh phasing relationships in planetary and epicyclic gears". *Journal of Mechanical Design,* ***126***(2), Mar., pp. 365–370.